Identification and Characterization of Kinetically Competent Carbinolamine and α-Iminoglutarate Complexes in the Glutamate Dehydrogenase-Catalyzed Oxidation of L-Glutamate Using a Multiwavelength Transient State Approach†

Steven J. Maniscalco, Swapan K. Saha, and Harvey F. Fisher*

Laboratory of Molecular Biochemistry, VA Medical Center, Kansas City, Missouri 64128, and Department of Biochemistry and Molecular Biology, University of Kansas Medical Center, Kansas City, Kansas 66160-7421

Received April 23, 1998; Revised Manuscript Received August 5, 1998

ABSTRACT: A highly constrained and heavily overdetermined multiwavelength transient state kinetic approach has been used to study the oxidative deamination of L-glutamate catalyzed by beef liver glutamate dehydrogenase. Spectra generated using the known enzyme-reduced coenzyme−substrate spectrum served as models for deconvolution of kinetic scan data. Deconvolution of the multiwavelength time course array shows formation of three distinguishable intermediates in the reaction sequence, an ultrablue-shifted complex, an ultrared-shifted complex, and a blue-shifted complex. The ultrablue-shifted entity is identified as the enzyme−NADPH−α-iminoglutarate complex (ERI) and the ultrared as the enzyme−NADPH−α-carbinolamine complex (ERC). The blue-shifted complex is characterized as the E−NADPH−ketoglutarate species (ERK). The location of these species along the reaction coordinate has been determined and their kinetic competency in the reaction sequence has been established by fitting the concentration time courses of the components for both the α-deuterio- and the α-protio-L-glutamate reactions to the now highly constrained differential equations derived from a kinetic scheme involving the sequential formation of α-iminoglutarate, α-carbinolamine, and α-ketoglutarate-reduced coenzyme complexes, following the formation of two prehydride transfer complexes.

The application of the steady state kinetic approach has provided the basis for much of our current understanding of the mechanisms of enzymatic catalysis. While having the advantage of providing rigorous equations for complex reaction schemes, it is limited in its ability to identify and distinguish between the various control complexes whose successive formation and subsequent interconversions form the heart of these complex mechanisms. The transient state stopped flow approach, on the other hand, offers the advantage of real-time observation of these events, but is itself limited by the lack of availability of a rigorous mathematical approach that can be applied to systems of realistic complexity. While transient state phenomena can always be fitted by any of a number of "simulation" computer programs, such solutions are not unique at best and, if not severely constrained, may be quite misleading if not actually false. The development of commercially available instrumentation now permits the acquisition of very good quality multiwavelength time courses. Commercial global spectral fitting programs are available for resolving such data into spectral components and their time courses. However, we found that such programs require extremely close estimates of the input rate constants, without which incorrect solutions may result.[1] Here we develop a procedure which does have the ability to resolve such a data-dense absorbance versus time and wavelength array into kinetically competent individual component time courses. This procedure, which uses a simultaneous solution for reactions with both deuterium-substituted and nonsubstituted components, provides the constraints on model-fitting algorithms needed to establish the kinetic competence of individual enzyme intermediate complexes in occupying designated positions in a detailed reaction time course.

EXPERIMENTAL PROCEDURES

Materials. Beef liver glutamate dehydrogenase obtained from Sigma as an ammonium sulfate suspension was dialyzed against three changes of 0.1 M phosphate buffer at the required pH, and was filtered through Norit A and a 0.45 μm filter. The concentration of the enzyme was measured spectrophotometrically at 280 nm ($\epsilon = 54\,400$ mM^{-1} cm^{-1}). $NADP^+$ and glutamic acid were purchased from Sigma and Calbiochem, respectively, and were used without any further purification. L-[α^2-H]Glutamic acid was prepared following the method of Rife and Cleland (*1*). NMR analysis of the

† This work was supported in part by the Department of Veterans Affairs and by Grant MCB-9513398 from the National Science Foundation.

* Address correspondence to this author at Research Service, VA Medical Center, 4801 Linwood Blvd., Kansas City, MO 64128. Telephone: (816) 861-4700, ext 7156. Fax: (816) 861-1110.

[1] This problem is particularly severe with systems where the spectral separation of individual components does not vary widely, and where the input data have reasonable amounts of noise associated with it. In simulated systems, we have observed that an apparent solution is often obtained, but gives totally incorrect answers. We will present a more detailed analysis of the validity and degree of uniqueness of fitting mathematical "models" to transient state kinetic measurements elsewhere.

S0006-2960(98)00923-4 CCC: $15.00
Published on Web 09/26/1998

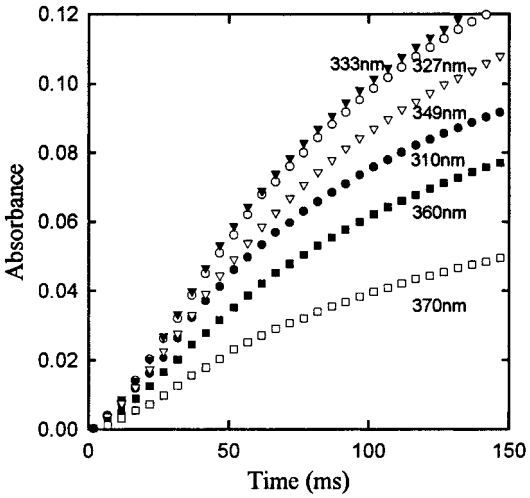

FIGURE 1: Selected individual fixed-wavelength slices of the multiwavelength absorbance time course array of the bovine liver glutamate dehydrogenase-catalyzed reaction. The wavelength time course points are shown at some selected wavelengths.

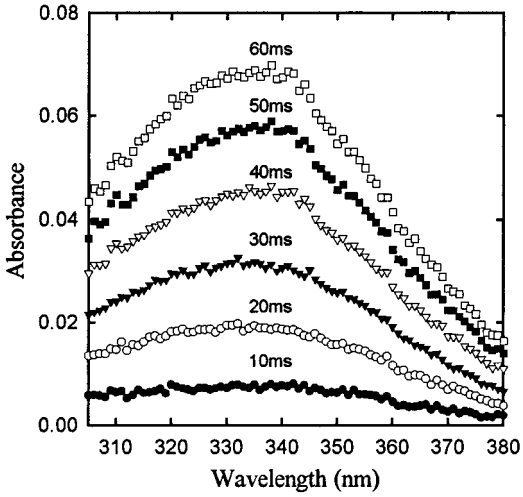

FIGURE 2: Selected individual fixed-time spectra of the multiwavelength absorbance time course array collected at 0.5 ms intervals. Those shown here differ by 10 ms intervals from 5.4 to 65.4 ms.

deuterated glutamic acid showed 100% conversion at the α-position.

Transient State Kinetics. The transient state absorbance versus wavelength and time array was obtained using a Applied Photophysics SX-17MV stopped flow apparatus equipped with dual monochromators by assembling a series of side-by-side single-wavelength time traces, in which a solution containing enzyme and L-glutamate in one syringe is mixed with a solution containing NADP and enzyme in the other. The apparatus then purges the system, advances to the next wavelength, resets its photomultiplier voltage automatically to a value determined from an enzyme−NADP mixing reference experiment all under computer control, and triggers the next shot. The spectra were collected at 1 nm and 0.5 ms intervals. An individual experiment such as that portrayed in Figure 1 takes approximately 20 min to produce an array comprising 30 500 individual points, each of which is an average of three successive photomultiplier readings. The reaction was carried out at 10 °C in a 0.1 M phosphate buffer (pH 7.2). The reactant concentrations after mixing were 45 μM E,[2] 380 μM NADP, and 45 mM L-glutamate. To eliminate the effects of time-dependent changes in light scatter due to dilution, the same concentration of enzyme was maintained in both syringes containing the reactants. The fluorescence measurements were taken under the same conditions as those taken with absorbance with a 340 nm excitation wavelength and using a GG455 filter placed after the cuvette.

The spectral data were analyzed using two commercially available programs, Matlab 5.1 and Scientist 2.01. Matlab 5.1 has been used to deconvolute the scan data by solving the data matrixes with known vectors (component spectra matrixes). Scientist 2.01 was used to fit the deconvoluted spectral components to the differential equations derived from the kinetic scheme solving for the rate constants corresponding to each step. A Jacobian matrix was generated from the analytic forms of the partial derivatives with respect to time. Treating the Jacobian matrix as banded, we used variable-coefficient Backward Differentiation Formula and Adams-Moulton methods in Nordsieck form to solve the rate constants. The technique is described by G. Byrne and A. Hindmarsh in EPISODE: An experimental package for the integration of systems of ordinary differential equations with banded Jacobians [Lawerence Livermore National Laboritory Report UCIS-30132, Livermore, (http://www.micromath-.com/index.html); Scientist, version 2.01].

RESULTS AND DISCUSSION

The oxidative deamination of L-glutamate to α-ketoglutarate and ammonia as catalyzed by bovine liver glutamate dehydrogenase is currently understood to involve the following steps (*2*−*6*):

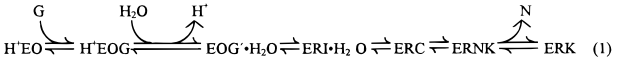

(1)

where E is the enzyme, O is NADP, G is L-glutamate, R is NADPH, I is α-iminoglutarate, C is the carbinolamine form, N is ammonia, and K is α-ketoglutarate.[3]

Figures 1 and 2 show representative portions of an array which contains the complete multiwavelength spectroscopic time course of the early portion of the reaction shown in eq 1. Figure 1 shows several selected constant-wavelength time courses. Figure 2 shows the spectra of the reaction mixture at some selected times.

The analysis of this array involves three successive processes: (1) the qualitative and quantitative deconvolution of each observed spectrum (time slices of the array) into the individual components with a known shape and extinction coefficient whose individual contributions account for the

[2] Abbreviations: b1GDH, bovine liver glutamate dehydrogenase; E, enzyme; O, oxidized coenzyme (NADP); R, reduced coenzyme (NADPH); I, α-iminoglutarate; C, α-carbinolamine; K, α-ketoglutarate; N, ammonia.

[3] The reaction actually observed at the high concentrations of L-glutamate used in our studies proceeds through some additional steps ERK + G ⇌ ERG + K and, eventually, to the release of free R and K. Since the step involving the replacement of K by G is very slow ($t_{1/2}$ = 1.7 s), ERG, ER, and R do not appear in the time range studied here (*7*). Since the final portion of the reaction is well understood and does not involve any covalent bond-breaking events, we have not considered it here, beyond the use of the known spectra of these enzymes as spectroscopic reference models.

observed signal, (2) the assignment of each of these components to a known or postulated reactive enzyme complex, and (3) the determination of the kinetic competence of each of these species in occupying their postulated positions along the reaction time course. We now proceed to describe the method, application, and results of each of these processes in turn.

Deconvolution of Fixed-Time Spectra into Reaction Component Concentrations. To avoid the creation of artificial spectral components that do not correspond to those of existing reaction complexes, we impose the following restrictions on our analysis: each component spectrum must either represent that of some known entity or be able to be derived from that of the reduced nicotinomide chromophore by some operation which has a known and previously demonstrated physical basis. We have found that the spectrum of any given reduced nicotinomide moiety essentially retains its shape and exhibits only minor changes in its extinction coefficient (*8*) regardless of the particular enzyme complex in which it occurs. Such spectra do, however, undergo substantial shifts along the wavelength axis from the uncomplexed form. Those complexes of b1GDH whose spectra and extinction coefficients have been rigorously established include ER and ERG (λ_{max} = 342 nm), ERK (λ_{max} = 333 nm), and free R (λ_{max} = 339 nm). Free O, HEOG, and the fluorescent EOG′ complex have been shown not to provide significant absorbance contributions in the spectral range of interest here. We have recently reported spectroscopic evidence of the existence of an additional reactive intermediate complex in the blGDH-catalyzed reaction (*9*). A transient state study of the reverse direction of the reaction shown in eq 1 indicated the accumulation of a component whose spectrum was nearly identical in shape to that of the ERK complex but whose maximum absorbance was shifted to an even lower wavelength (327 nm), and is thus designated as an "ultrablue-shifted" entity. Since the only phenomena observed in the reverse direction under these conditions were the appearance of the ultrablue-shifted complex and the concomitant disappearance of free NADPH, whose molar absorbance coefficient is known to be 6.22×10^6, the corresponding value for the ultrablue intermediate was determined to be 6.0×10^6. While this new intermediate appeared to occur on the reduced coenzyme side of the hydride transfer step, its precise location along the reaction coordinate could not be assigned from the evidence at hand. This spectrum provides an additional potential component which we can use in the spectral resolution step of our overall analytical paradigm. The spectra of the pertinent known glutamate dehydrogenase complexes are shown in Figure 3A. To aid in the resolution process, individual time-slice spectra are first "pinned" by subtracting the absorbance spectrum taken at 1.1 ms, a point in time at which complex formation is quantitatively negligible.

To carry out a resolution involving a variety of possible components for a set of 394 individual spectra, we have developed the following procedure which makes use of a reiterative computer-run matrix operation.

According to Beer's law, $A_{\lambda,t}$, the observed absorbance at a given wavelength and at a given time, is derived from

$$A_{\lambda,t} = a_\lambda[\mathrm{A}]_t + b_\lambda[\mathrm{B}]_t + c_\lambda[\mathrm{C}]_t + \ldots \qquad (2)$$

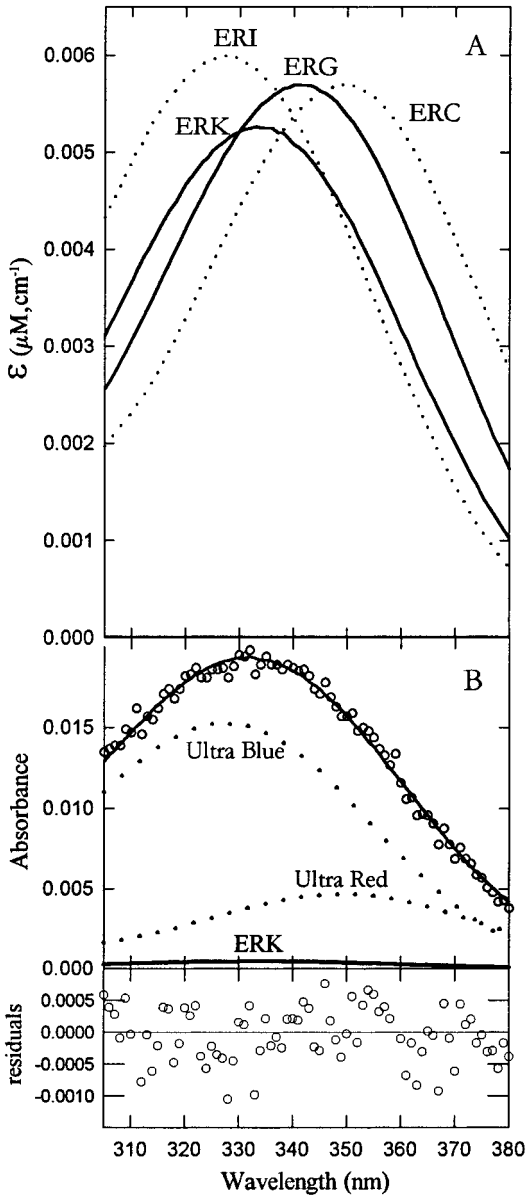

FIGURE 3: Resolution of fixed-time absorbance time slices of the array. (A) Model component spectra used in the analysis. Spectra corresponding to previously known entities (ERG and ERK) are indicated by solid lines. Spectra of species found in the course of this work (those of ERI and ERC) are indicated by dotted lines. (B) Typical deconvolution of a spectrum into components.

where $[\mathrm{A}]_t$, $[\mathrm{B}]_t$, and $[\mathrm{C}]_t$ represent the molar concentrations of species A, B, and C at any given time and a_λ, b_λ, and c_λ are the molar absorbance coefficients for these species at a given wavelength, respectively. We can therefore resolve the observed spectrum for any give value of t by applying Cramer's rule to a determinant of the form

$$\begin{vmatrix} a_{305} & b_{305} & c_{305} & A_{305} \\ a_{306} & b_{306} & c_{306} & A_{306} \\ \ldots & \ldots & \ldots & \ldots \\ a_{380} & b_{380} & c_{380} & A_{380} \end{vmatrix} = 0 \qquad (3)$$

To the extent that the model component spectra provided are correct in absorbance coefficients and in wavelength maxima, the solution of this determinant provides the values of the molar concentrations, [A], [B], [C], etc., at a single point in time, t. Where this procedure using known

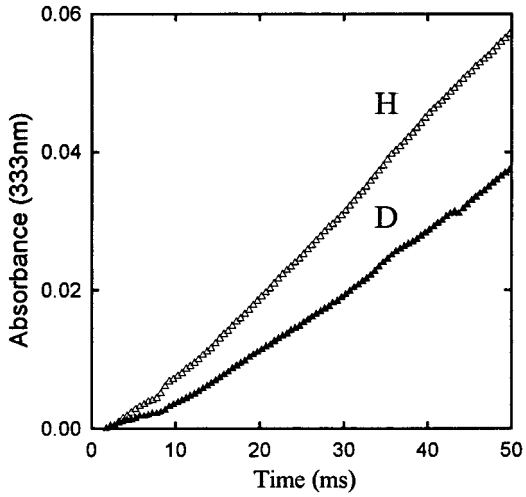

FIGURE 4: Comparison of 333 nm time courses of the α-deuterio-glutamate reaction (△) with those of the unsubstituted substrate reaction (▲).

complexes fails to account for the observed spectral time slices, we can infer the presence of complexes whose spectra differ from those of previously known forms. These new spectral components are then synthesized according to the rules described above, shifting the known intermediate complex's spectral shape to some wavelength which levels the residual difference spectrum. (Here, a normal enzyme−NADPH−ketoglutarate complex is used to synthesize the ultrablue complex and the enzyme−NADPH−glutamate complex to synthesize the ultrared complex.) Various models were generated and used as component vectors to solve the matrix produced by the experimental data. The best fits were judged from the degree of flatness of residuals along the wavelength axis. Application of this procedure showed the necessity of including a substantial contribution of the ultrablue-shifted component described above. This entity, already identified in the reverse reaction, has not previously been reported in the forward reaction. The "normal" red-shifted component (λ_{max} = 342 nm), which characterizes the spectra of the ER and ERG complexes, does not appear to make any significant contribution to the observed spectra in the time range studied here.[3] However, the analysis did result in the discovery of a spectroscopic previously unreported entity shown in Figure 3B. This component has a λ_{max} of 351 nm and is thus red-shifted recognizably further than the previously identified ERG complex, and is therefore designated as the "ultrared" component. The normal blue component, identical to the spectrum of the ERK complex, appeared distinctly in the spectra observed in the later portion of the time period. The component analyses for a substantial number of these time-slice spectra plotted versus time are presented in Figure 5.

Resolution of the experimental data of Figure 2 revealed three easily distinguishable components: (1) an ultrablue-shifted component which exhibited a rapid burst phase, (2) an ultrared-shifted component which shows a brief initial lag, followed by an increase which reaches a steady state at later times, and (3) a component having a blue-shifted spectrum identical to that of ERK which appears only after a long lag period and continues to increase throughout the time course. This qualitative observations indicate that the ultrablue species is the first intermediate formed during the reaction. Following the appearance of the ultrablue complex, an ultrared species is formed which is then followed by the formation of the normal blue-shifted species. We have already identified the normal blue-shifted species as ERK (8). Thus, according to the reaction scheme, the ultrablue-shifted species should correspond to the formation of ERI, and would appear to be competent in producing the ultrared-shifted ERC species (Figure 3A). Therefore, we write a provisory scheme and assign the spectral components to those species in the following way:

$$\underset{\text{colorless}}{\text{HEOG}} \overset{k_1}{\underset{k_2}{\rightleftharpoons}} \underset{\text{ultrared}}{\text{EOG}'} \overset{k_3}{\underset{k_4}{\rightleftharpoons}} \underset{\text{ultrablue}}{\text{ERI}} \overset{k_5}{\underset{k_6}{\rightleftharpoons}} \underset{\text{ultrared}}{\text{ERC}} \overset{k_7}{\underset{k_8}{\rightleftharpoons}} \underset{\text{blue}}{\text{ERK}} \quad (4)$$

The following series of differential equations describe the time-dependent behavior of such a reaction:

$$d[HEOG]/dt = k_2[EOG'] - k_1[HEOG] \quad (5)$$

$$d[EOG']/dt = k_1[HEOG] + k_4[ERI] - (k_2 + k_3)[EOG'] \quad (6)$$

$$d[ERI]/dt = k_3[EOG'] + k_6[ERC] - (k_4 + k_5)[ERI] \quad (7)$$

$$d[ERC]/dt = k_5[ERI] + k_8[ERK] - (k_6 + k_7)[ERC] \quad (8)$$

$$d[ERK]/dt = k_7[ERC] - k_8[ERK] \quad (9)$$

Substituting the values of [ERI], [ERC], and [ERK] determined from the spectral resolution process at each specific value of *t*, we obtain a system of equations which can be solved numerically for the values of the individual rate constants by means described in Experimental Procedures. Applying this approach, we successfully solved a matrix of sets of eqs 5−9 taken at 394 individual times, and values for each of the eight rate constants were obtained. This mathematical convergence affords proof of the kinetic competence of the ultrared component in occupying a position between the ultrablue and the blue components on the reaction coordinate. However, solutions of matrixes of this sort, containing as they do multiple sources of both random and systematic errors, cannot be guaranteed to be unique. Their validity depends, in fact, on the number of independent constraints imposed on the solution. To increase the rigor of the test of the kinetic competence of eq 4 in representing the reaction, we have imposed a further constraint. We have carried out the reaction a second time under conditions identical to those reported, but using α-deuterio-L-glutamate as a substrate. A comparison of the observed signals of the two reactions at a single wavelength is shown in Figure 4. The data from this experiment were treated in the same manner as those of the experiment with the nonisotopically substituted components. Some typical pairs of reaction time courses for each of the components from the two experiments are shown in Figure 5. It may be noticed that the behavior of the transient state kinetic isotope effects indicates that all three components must be post-hydride transfer species according to the rules for such effects we have described previously (*10*).

Both the protio- and the deuterio-L-glutamate data sets converged when solved separately, but the corresponding rate constants from the two sets did not agree well. According to the chemistry described in eq 4, only k_3 and k_4 (the two

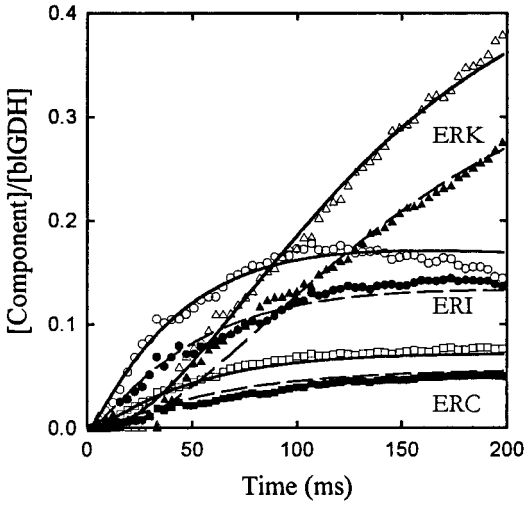

FIGURE 5: Component concentrations plotted vs time. The open symbols represent data from the L-[α-^{3}H]glutamate reaction, while the solid symbols represent data for the corresponding complex in the *d*-D-L-glutamate. The complexes are ERI (○ and ●), ERC (□ and ■), and ERK (△ and ▲). The solid lines represent the best fit of the simultaneous solution of eqs 5−9 and the corresponding set of equations for the isotopically substituted substrate. The individual rate constants are as follows: $k_1 = 14 \pm 3\ s^{-1}$, $k_2 = 0.1 \pm 5\ s^{-1}$, $k_3 = 120 \pm 30\ s^{-1}$, $k_4 = 220 \pm 100\ s^{-1}$, $k_5 = 130 \pm 24\ s^{-1}$, $k_6 = 290 \pm 60\ s^{-1}$, $k_7 = 67 \pm 3\ s^{-1}$, and $k_8 = 10 \pm 1\ s^{-1}$, where the errors are expressed as the univariate confidence range. The rate constants used for the reaction with the isotope-substituted components are the same except for the two involved in the hydride transfer step, where $k_{3i} = 54 \pm 11\ s^{-1}$ and $k_{4i} = 180 \pm 80\ s^{-1}$ were found.

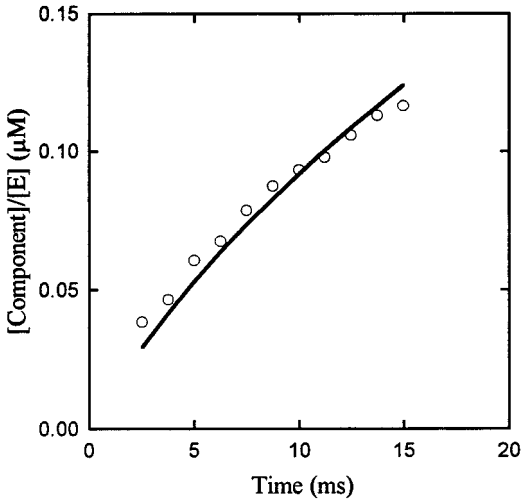

FIGURE 6: Time courses of the 340 nm excited fluorescence (○) and [EOG′] (−) calculated from the kinetic model. The solid line represents the time course of the fluorescent charge-transfer EOG′ complex predicted using the rate constants listed in the legend of Figure 5. The open circles represent the 340 nm excited fluorescence signal expressed in molar units scaled by an arbitrarily assumed fluorescence coefficient. Both the predicted curve and the experimental results for this very early time period for reactions with both the isotopically substituted and nonsubstituted components were indistinguishable.

constants involved in hydride transfer) are permitted to vary. Imposing this extremely strict constraint, we proceeded to solve the two data sets simultaneously.

The results are shown in Figure 5. A satisfactory agreement between the experimental data and the time courses of the individual components of reactions with both the deuterio-substituted and the unsubstituted components calculated from the appropriately modified form of eqs 5−9 proves the kinetic competence of the components in the reaction scheme shown in eq 4.[4] The rate constants for the individual steps are shown in the legend of Figure 5.[5]

An independent confirmation of the validity of the assignments we have made is provided in Figure 6, where we have plotted the measured 340 nm excited fluorescence of a reaction identical to that shown in Figure 5 for both the α-protio- and α-deuterio-L-glutamate reactions. We have previously shown that the EOG′ species is a weakly absorbing but highly fluorescent prehydride charge-transfer complex (*5*). We also know that the normal fluorescence of NADPH is completely quenched in the ERK complex. The fluorescent properties of NADPH in ERI and ERC are not known at this time, but their concentrations are negligible in the initial phase of the reaction. On this basis, we have fitted the fluorescence signal to this phase of the [EOG′] curve, by again solving eqs 5−9 with all eight rate constants fixed at the values shown in the legend of Figure 5 and assuming an arbitrary fluorescence coefficient. Both the theoretical curve and the experimental fluorescence data for reactions with the isotopically substituted and the unsubstituted components were indistinguishable, proving that the measured signal must be due solely to a pre-hydride transfer complex (*10*). The fit agrees sufficiently well to support the general features of the scheme we have described,

[4] The discrepancies between the individual theoretical curves and the component concentrations for the individual time courses require some comment. Single-wavelength time courses (such as those shown in Figure 1) can be fitted with great precision with simple double-exponential equations, but the parameters so obtained, by themselves, provide no useful mechanistic information. In turn, each of the sets of resolved components shown in Figure 5 could be fitted individually with quite good precision, but the results of such an unconstrained fitting procedure are found to be mutually inconsistent. The well-constrained solution using eqs 5−9, for the two reactions (deuterio or protio substrates) must necessarily provide somewhat poorer fits since they are forced to agree on a common set of values for each individual rate constant for a given reaction. Solving both the deuterio and protio reaction matrixes simultaneously effectively doubles the number of constraints on the solution, producing again a necessarily even less aesthetic fit of the data points to the curves than those of the separate solutions, but gaining enormously in the rigor of the proof and the believability of the ERI rate constants.

[5] Although the set of individual rate constants listed in the legend of Figure 5 provide a fit to the proposed kinetic scheme sufficient to prove the kinetic competence of the central ERI ⇌ ERC ⇌ ERK interconversions, the nature of the mathematical process by which they were calculated suggests that the specific values for at least some of these constants should be viewed with some degree of skepticism. The values of k_5, k_6, k_7, and k_8 relate to directly observed phenomena and are, therefore, quite probably reliable within their stated error limits. The other rate constants, however, are inferred from the behavior of the system as a whole, and may or may not represent a unique set of values. The ratios k_3/k_{3i} and k_4/k_{4i} (where k_{3i} and k_{4i} represent the rate constants for reaction with the deuterio-substituted components corresponding to k_3 and k_4, respectively, in the reaction with the unsubstituted components) listed indicate substantial primary kinetic isotope effects in both directions. While the cumulative effects of the individual errors in the individual constants preclude any reliable estimate of the precise values of the KIEs, it is clear that the intrinsic KIE for hydride transfer in the forward direction must be less than 3, in agreement with the value reported in ref *9*, which was obtained by a different approach. Since neither of these two methods is subject to kinetic masking effects, we conclude that the transition state, viewed from the forward direction, must be distinctively product-like.

although the deviations indicate some additional complexity in both the initial and the very late stages of the reaction.[4]

Indirect evidence from O^{18} exchange studies implicated the involvement of an enzyme α-iminoglutarate−NADPH complex (ERI) as an obligatory intermediate in this reaction (*11*), and chemical necessity appeared to dictate the requirement of the formation of an α-carbinolamine complex (ERC) as an ensuing step. However, the findings presented here offer the first direct physical evidence of the actual occurrence of these two postulated entities. The ability to track these two new intermediate forms by direct observation offers the opportunity to study the chemistry of their formation and interconversion at a more fundamental level than has been previously possible.

It can be seen from eq 4 that red- and blue-shifted complexes appear to alternate along the reaction coordinate. This pattern is in fact continued with the formation of the red-shifted ERG complex formed from the blue-shifted ERK complex (not shown in eq 4). The directions of these shifts do correlate in every case with the state of hybridization of the α-carbon atom of the substrate or its analogue. This correlation is shown in eq 10.

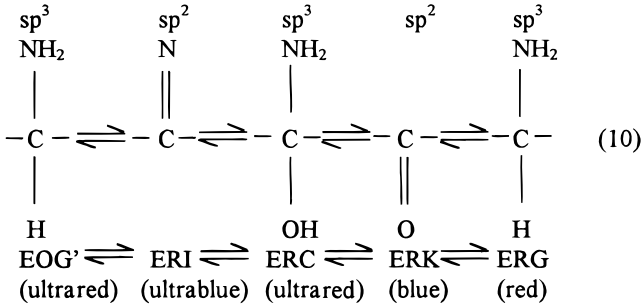

(10)

It can be seen that only complexes which involve a ligand sp^2 α-carbon atom undergo a blue shift of some magnitude and that all complexes which involve an sp^3 ligand α-carbon atom undergo a red shift. This case is strengthened by the fact that all known complexes of this and of the analogous (but not identical) reaction catalyzed by clostridium symbiosum glutamate dehydrogenase behave in precisely the same fashion. While we are not aware of any theoretical basis that would explain this pattern, it would seem reasonable to suspect that these opposing shifts may be due to effects on the dipole moment of the reduced nicotinamide chromophore induced by the necessarily different geometrical loci of the sp^2 and sp^3 orbitals. Whatever the explanation, however, the phenomenological correlation shown in eq 10 would appear to add some additional support to the correlation between the spectroscopically observed entities and the corresponding chemical species we have postulated.

The work described here offers a general approach to the proof of chemical mechanisms from transient state kinetic data. Its principal advantage over previous approaches lies in the relatively high degree of rigor it affords. That parameter depends on the number of equations that can be included in the solution to the set of differential mechanisms required to describe a particular postulated mechanism, and even more on the degree of mutual independence of those equations. In the formal approach described here, it is relatively simple to increase that degree of rigor by introducing further and more independent equations based on the deconvoluted time-courses of other more specific optical phenomena, such as indicator dye proton release and various fluorescence phenomena. Thus, this approach should be quite generally applicable to the study of any other enzyme system whose reaction time course produces optically observable phenomena.

REFERENCES

1. Rife, J. E., and Cleland, W. W. (1980) *Biochemistry 19*, 2328−2333.
2. Brunhuber, N. M., and Blanchard, J. S. (1994) *Crit. Rev. Mol. Biochem. 29*, 415−467.
3. Lilley, K. S., and Engel, P. C. (1992) *Eur. J. Biochem. 207*, 533−540.
4. Narinder, S., Maniscalco, S. J., and Fisher, H. F. (1993) *J. Biol. Chem. 268*, 18−21.
5. Saha, S. K., Maniscalco, S. J., Singh, N., and Fisher, H. F. (1994) *J. Biol. Chem. 269*, 29592.
6. Saha, S. K., Maniscalco, S. J., and Fisher, H. F. (1996) *Biochemistry 35*, 16483−16488.
7. Fisher, H. F., Pazhanisamy, S., and Medary, R. T. (1987) *J. Biol. Chem. 262*, 11684−11687.
8. Cross, D. G. (1972) *J. Biol. Chem. 247*, 784−789.
9. Saha, S. K., Maniscalco, S. J., and Fisher, H. F. (1998) *Biochim. Biophys. Acta 1382*, 8−12.
10. Fisher, H. F., and Saha, S. K. (1996) *Biochemistry 35*, 83−88.
11. Fisher, H. F., and Viswanathan, T. S. (1984) *Proc. Natl. Acad. Sci. U.S.A. 81*, 2747−2751.

BI980923V